

Observation of three-neutron sequential emission from $^{25}\text{O}^*$

C. Sword,¹ J. Brett,¹ T. Baumann,² B. A. Brown,^{2,3} N. Frank,⁴ J. Herman,⁴ M. D. Jones,⁵ H. Karrick,⁴ A. N. Kuchera,⁶ M. Thoennessen,^{2,3,*} J. A. Tostevin,⁷ M. Tuttle-Timm,⁴ and P. A. DeYoung^{1,†}

¹*Department of Physics, Hope College, Holland, Michigan 49423, USA*

²*National Superconducting Cyclotron Laboratory, Michigan State University, East Lansing, Michigan 48824, USA*

³*Department of Physics and Astronomy, Michigan State University, East Lansing, Michigan 48824, USA*

⁴*Department of Physics, Augustana College, Rock Island, Illinois 61201, USA*

⁵*Department of Physics and Astronomy, University of North Carolina, Chapel Hill, North Carolina 27599, USA*

⁶*Department of Physics, Davidson College, Davidson, North Carolina 28035, USA*

⁷*Department of Physics, University of Surrey, Guildford, Surrey GU2 7XH, United Kingdom*



(Received 10 April 2019; published 26 September 2019)

Background: Measurements of neutron-unbound states can test nuclear models in very neutron-rich nuclei that, in some cases, cannot be probed with other methods.

Purpose: Search for highly excited neutron-unbound states of ^{25}O above the three-neutron separation energy.

Method: The decay energy of ^{25}O was reconstructed using the invariant mass spectroscopy method. A 101.3-MeV/u ^{27}Ne beam collided with a liquid-deuterium target. Two-proton removal reactions populated excited ^{25}O that decayed into three neutrons and an ^{22}O fragment. The neutrons were detected by arrays of plastic scintillator bars, whereas a 4-Tm dipole magnet placed directly after the target redirected charged fragments to a series of charged-particle detectors. The data were compared with detailed Monte Carlo simulations of the reaction process and subsequent decay.

Results: The data show evidence of neutron-unbound level(s) in ^{25}O at an excitation energy of about 9 MeV which decay sequentially by the emission of three neutrons to ^{22}O .

Conclusion: The observation of resonance strength in ^{25}O at about 9 MeV is consistent with shell-model and eikonal calculations for the two-proton removal reaction from ^{27}Ne .

DOI: [10.1103/PhysRevC.100.034323](https://doi.org/10.1103/PhysRevC.100.034323)

I. INTRODUCTION

The study of exotic nuclei beyond the drip lines is instrumental in exploring the validity of nuclear structure models in the neutron- and proton-rich regions of the nuclear chart. In particular, these models must describe the sudden change in the location of the neutron drip line for oxygen and fluorine [1]. Discovery of states beyond the drip line in these elements constrains model parameters and improves predictions of other states. For example, a measurement of the unbound ground state of ^{25}O , which decays by single neutron emission to the ground state of ^{24}O , placed limits on theoretical predictions for the particle stability of ^{26}O [2]. Since then, the unbound ground state of ^{26}O was discovered [3], and the most recent and precise measurement of its decay energy is 18 ± 3 (stat) ± 4 (syst) keV [4].

Although unbound excited states have been discovered in ^{23}O [5–7], ^{24}O [8–12], and even ^{26}O [4], a recent search for unbound excited states in ^{25}O was unable to confirm the observation of any excited states. The data were consistent with a state at about 3.3 MeV, but only an upper limit for the population of such a state was determined [13].

Figure 1 compares the measured excited states of ^{23}O , ^{24}O , and ^{25}O to results of calculations with the Gamow shell model using the density-matrix renormalization-group (GSM-DMRG) method [13] and a continuum shell model (CSM) [14]. The unconfirmed excited state from Ref. [13] is shown as a dashed line. Also of note in Fig. 1 are the levels above the ^{25}O three-neutron separation energy that should play a role in the decay of highly excited levels of ^{25}O via the emission of three neutrons. In ^{23}O and ^{24}O , these are the states at about 50 and 700 keV above the three-neutron separation energy, respectively [15].

The search for excited states by Jones *et al.* [13] was motivated by the prediction of low-lying intruder states from the pf shell due to the nearby island of inversion [16,17]. The experiment utilized the $^{24}\text{O}(d, p)$ transfer reaction to attempt to populate these states, but no evidence for any low-lying excited states was observed.

As shown in Fig. 1, there are excited states predicted by GSM-DMRG and CSM at or above the two-neutron separation energy (S_{2n}) that would decay by the emission of two (low-energy) neutrons. However, the fragment acceptance of the experiment of Jones *et al.* did not cover ^{23}O fragments from the (d, p) reaction. The present paper is based on a second beam ^{27}Ne , that was simultaneously transported to the target along with ^{24}O . Neutrons from the ^{27}Ne beam were detected in coincidence with ^{22}O fragments, thus, offering the opportunity to search for highly excited states of ^{25}O

*Present address: American Physical Society, Ridge, New York 11961, USA.

†deyoung@hope.edu

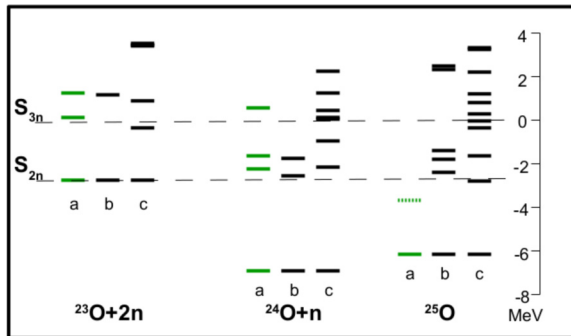


FIG. 1. Experimental [(a), green online] and theoretical (b) and (c) ground and excited states of ^{23}O , ^{24}O , and ^{25}O . The dashed lines correspond to the two- (S_{2n}) and three-neutron (S_{3n}) separation energies for ^{25}O . The theoretical levels shown in columns (b) and (c) are from Refs. [13,14], respectively. The experimental values were taken from the unevaluated data compilation XUNDL [15]. The unconfirmed excited state from Ref. [13] is shown as a dotted line.

above the three-neutron separation energy (S_{3n}) populated in the two-proton removal reaction. The feasibility to reconstruct excited states decaying by the emission of three or even four neutrons was demonstrated for the decay of excited states in ^{15}Be [18] and in the search of ^{12}He [19], respectively.

II. EXPERIMENTAL PROCEDURE

The measurement was performed at the National Superconducting Cyclotron Laboratory (NSCL) at Michigan State University. Secondary beams of neutron-rich nuclides were produced by fragmentation of a 140-MeV/u ^{48}Ca primary beam accelerated by the Coupled Cyclotron Facility and separated by the A1900 Fragment Separator. The secondary beam was composed mainly of 83.3-MeV/u ^{24}O ($\sim 30\%$) and 101.3-MeV/u ^{27}Ne ($\sim 40\%$) nuclei. The remainder of the beam was composed of light nuclei. Beam particles collided with the Ursinus College liquid deuterium [(LD) where D denotes ^2H] target which had an effective thickness of 650 mg/cm 2 [20,21]. The detector layout is shown in Fig. 2. Charged fragments were redirected by a 4-Tm large-gap superconducting dipole magnet (Sweeper) into two 30 \times 30 cm 2 position-sensitive cathode-readout drift chambers (CRDCs), that measure the trajectories of charged particles after the Sweeper. The charged fragments then entered a 65-cm-long ionization chamber (IC), which measured the energy loss of the fragments to determine their atomic number. A 4.5-mm plastic scintillator behind the IC, fragment scintillator (FSC), in combination with a 0.42-mm scintillator placed before the target, target scintillator (TSC), measured the time-of-flight (ToF) for each charged fragment.

Neutrons emitted in coincidence with oxygen fragments were detected by the Modular Neutron Array (MoNA) and Large multi-Institutional Scintillator Array (LISA). MoNA and LISA are configurable arrays of 2-m-long plastic scintillator bars that detect beam-velocity neutrons. In this experiment, 13 layers of 16 bars each were centered along the beam axis at distances of > 7.74 m from the target, and five layers were placed at 22° at distances of > 6.73 m. The position of interac-

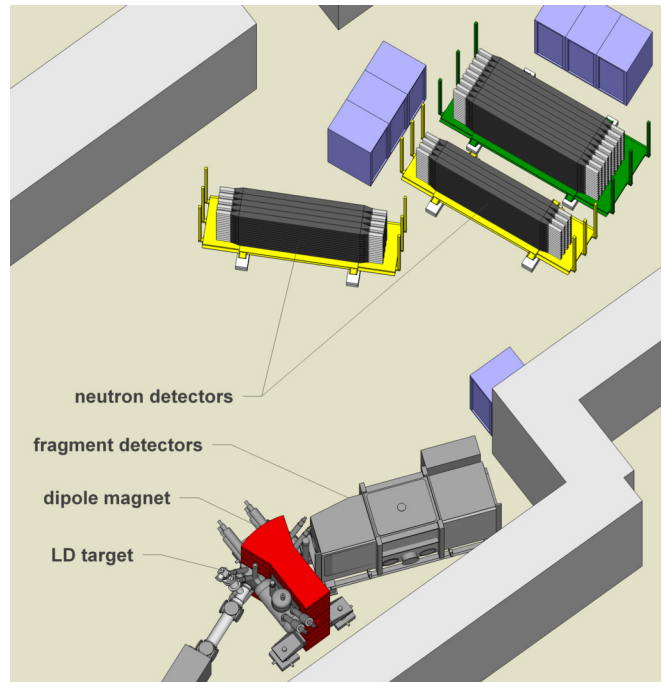


FIG. 2. Layout of detectors, Sweeper magnet, and target in the NSCL experimental area.

tion points along the beam and vertical axes were determined by the 10-cm thickness of each bar. The horizontal position was determined by the time difference between signals read out by photomultiplier tubes (PMTs) placed at each end of the scintillating bars. A simulation for three-neutron detection that includes geometrical acceptances, the actual detector positions, and neutron detection probabilities, indicates an efficiency of $\sim 4\%$ for the sequential decay described below.

Additional details can be found in Refs. [11,20] which report the results from the ^{24}O beam. The present analysis focuses on the data collected from the ^{27}Ne beam. One difference between this paper and that detailed in Ref. [20] is that it was not necessary to apply a charge threshold to the neutrons beyond the hardware threshold by constant fraction discriminators set at about 0.4 MeV.

III. DATA ANALYSIS

The incoming ^{27}Ne beam was selected event by event by ToF measurements between a scintillator located at the A1900 focal plane and the TSC. ^{22}O reaction products were then identified isotopically by energy loss in the IC, ToF between TSC and FSC, and the flight trajectory through the Sweeper as measured by the CRDCs.

The total mass of ^{25}O was calculated from the invariant of the sum of the energy-momentum four-vectors of an ^{22}O fragment and the three associated neutrons. The decay energy was then calculated from the difference between the reconstructed mass of $^{25}\text{O}^*$ and the sum of the masses of the three neutrons and the ^{22}O fragment. The kinematic properties of the detected neutrons were calculated from the measured interaction points in MoNA-LISA and from the ToF between the FSC and the

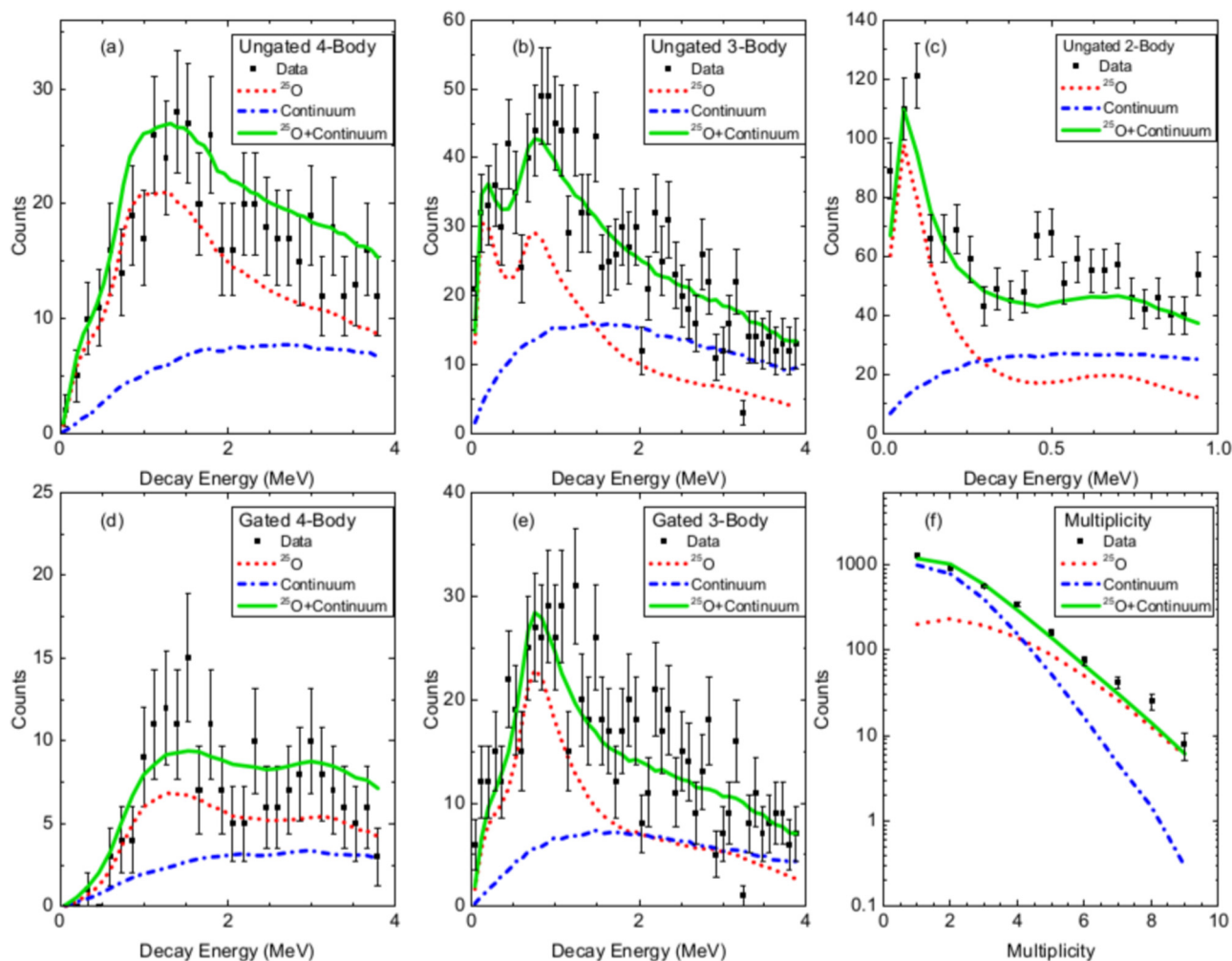


FIG. 3. Decay-energy (a)–(e) and hit-multiplicity (f) spectra of neutron(s) in coincidence with ^{22}O fragments. (a) Four-body ($^{22}\text{O} + 3n$), (b) three-body ($^{22}\text{O} + 2n$), and (c) two-body ($^{22}\text{O} + 1n$) decay-energy spectra are displayed in the top row. Neutron proximity-gated spectra for the four- and three-body decay energies are shown in panels (d) and (e), respectively. The experimental data (black points) are shown along with corresponding simulated data (solid green line) which are the sum of simulations of the three-neutron decay of ^{25}O (red dotted line) and continuum background contributions (blue dot-dashed line).

average of the two PMTs of a MoNA-LISA bar. Kinematic properties of ^{22}O fragments were calculated from an inverse transformation matrix constructed with COSY INFINITY [22,23] from the ion-optical properties of the Sweeper. This matrix maps kinematic measurements of the charged particles after the Sweeper to the kinematics at the position of the target.

The final four-body decay-energy spectra of ^{25}O decaying into ^{22}O and three neutrons calculated in this way are shown by the black points in Fig. 3(a). These data contain contributions from multiple interactions of the same neutron as well as contributions where a recoil proton deposits energy in two adjacent bars 10 cm apart. In previous experiments, for example, Ref. [18], causality gates set on the velocity and distance calculated between the interactions were used to reduce these contributions. Due to the limited statistics in the present experiment, only proximity gates were applied. These gates, requiring interactions in MoNA-LISA to be separated by more than 20 cm, suppressed events where scattered protons were registered in adjacent detector bars. The proximity-gated four-body spectrum is shown in Fig. 3(d). Although the

ungated spectrum exhibits only a peak at near 1.3 MeV, a second peak appears at about 3 MeV in the gated spectrum. The relative reduction of the prominence of the 1.3-MeV peak in the gated spectrum indicates that it might be due to events where the neutron from the decay of ^{24}O scatters in the arrays and is recorded twice. At the same time the emergence of the 3-MeV peak in the gated spectrum indicates that it corresponds to an excited unbound state in ^{25}O .

In addition to the four-body decay-energy spectra, further information can be extracted by reconstructing two- and three-body decay-energy spectra. These spectra can potentially exhibit unbound resonances in the subsystems of ^{24}O (three-body) and ^{23}O (two-body). This occurs if ^{24}O and ^{23}O are populated in the reaction directly, or if one or two of the three neutrons from the decay of ^{25}O are not detected. The MoNA-LISA and Sweeper system is most efficient for low decay energies so the decay-energy spectra will preferentially display low-energy resonances in the subsystems.

Indeed, the three-body decay-energy spectrum of ^{24}O , shown in Fig. 3(b), exhibits a peak due to the decay of a

state in ^{24}O located about 700 keV above the two-neutron separation energy. This is most likely the state reported in Refs. [9,11]. Similar to the four-body spectra described above, the enhancement at low decay energies is due to events where the neutron from the decay of ^{23}O scatters in the array and is recorded twice. This interpretation is confirmed by the proximity-gated three-body decay-energy spectrum where the low-energy peak due to the scattering events has been eliminated [see Fig. 3(e)].

Finally, the two-body decay-energy spectrum ($^{22}\text{O} + 1n$) clearly shows the low-energy resonance in ^{23}O first observed in Ref. [6]. In both this and the three-body decay, the data are adequately reproduced by a single broad resonant state at 3 MeV above the two-neutron separation energy. Note the expanded scale in Fig. 3(c).

The data cannot be directly compared to theoretical calculations because detector acceptances and resolutions have to be taken into account. Thus, detailed Monte Carlo simulations modeling different reactions populating excited states in the oxygen isotopes were performed. The properties of the incoming beam and the target thickness were input parameters. The outgoing fragment and neutrons from the simulated reaction in the target were tracked to the charged-particle detectors and MoNA-LISA, respectively. Interactions in MoNA-LISA were modeled with GEANT4 [24] coupled with MENATE_R [25] to properly account for the scattering in the array. Events falling within the geometric acceptances of the detectors were folded with the detector resolutions. Simulated two-, three-, and four-body decay-energy spectra were then reconstructed in the same way as the experimental data.

There are many different reaction channels available for a high-energy ^{27}Ne beam interacting with a liquid-deuterium target leading to a final ^{22}O fragment. Because the acceptance of the Sweeper was centered at (small) forward angles and the measured outgoing fragments were emitted essentially at the same velocity as the incoming beam, only peripheral collisions could contribute to the final measured spectra. Still there are many different reactions to consider, including two-proton removal to ^{25}O , $2p1n$ removal to ^{24}O , or $2p2n$ removal to ^{23}O . The latter oxygen isotope could also be directly populated by the removal of an α particle. All these reactions can possibly populate discrete low-lying resonances or unresolved highly excited states in the continuum of these nuclides.

A simulation was made of a sequential decay process based on a 3-MeV state in ^{25}O , a 700-keV state in ^{24}O , and a 50-keV state in ^{23}O (relative to the ^{25}O three-neutron separation energy). Also included in the model was a single-neutron emission (thermal) Maxwell-Boltzmann distribution to account for continuum background contributions. Reduced χ^2 fits were performed which included the five decay-energy spectra shown in Figs. 3(a)–3(e) and the overall neutron multiplicity spectrum, Fig. 3(f), to determine the scale factor of the two contributions, ^{25}O decay and background. The energies of the three states, excitation in ^{25}O and two intermediate levels were not varied in the fit.

Simulations that included significant contributions from the direct population of the discrete states in ^{23}O or ^{24}O could not reproduce the data. They failed to describe the relative strengths of the features in the three-body decay

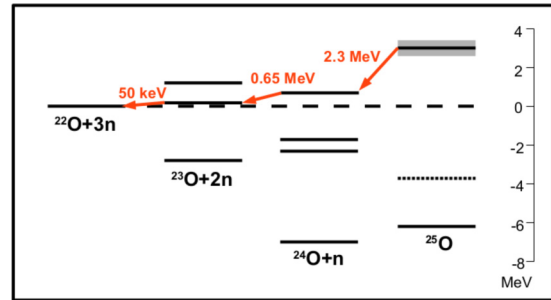


FIG. 4. Level diagram of the sequential emission of three neutrons from $^{25}\text{O}^*$ observed in this experiment. The levels shown are the same as the experimental levels presented in column (a) of Fig. 1. The gray box indicates the resonance strength from several levels observed in the present experiment. The arrows and energies (red) show the sequential transitions. The dashed line is the three-neutron separation energy. The unconfirmed excited state from Ref. [13] is shown as a dotted line.

energy spectra, Figs. 3(b) and 3(e), and the multiplicity spectrum, Fig. 3(f). The best fit to the data was achieved with simulations populating excited states in ^{25}O in combination with the continuum background contribution. The green solid lines in Fig. 3 show the results of the simulations including a resonance at 3-MeV decay energy in ^{25}O (red dotted lines). The background is shown by blue dot-dashed lines. The total decay energy of this resonance is measured with respect to the $^{22}\text{O} + 3n$ system and decays via a sequence of three neutrons with energies of 2.3 MeV, 0.65 MeV, and 50 keV as shown in Fig. 4. Adding the three-neutron separation energy of ^{25}O of about 6 MeV locates the state at an excitation energy of 9 MeV in ^{25}O .

IV. INTERPRETATION OF RESULTS

The observation of resonance strength at 9-MeV excitation energy is consistent with the presence of states in this area predicted by the GSM-DMRG [13] and the CSM [14] models as shown in Fig. 1. The CSM model also predicts several states just above the three-neutron separation energy at about 6 MeV. The eikonal model approach of Ref. [26] was used to calculate the probability for such states above the three-neutron separation energy to be populated in the direct two-proton removal reaction. The spectroscopic overlaps (two-nucleon amplitudes) of the $^{25}\text{O}^*$ final states were calculated with the shell-model code OXBASH [27]. The calculations included the first four major shells, including the $l = 3$, f shell, and both $0\hbar\omega$ and $1\hbar\omega$ transitions were allowed.

The calculations were made with the OXBASH code rather than the more recent NUSHELLX program [28]. The $1\hbar\omega$ restrictions require the use of basis states that have good isospin T that can be made with the OXBASH code. The NUSHELLX code uses a proton-neutron coupled basis where $\hbar\omega$ truncations can only be performed with protons and neutrons before they are coupled. A coupled basis that includes $1\hbar\omega$ for protons and $1\hbar\omega$ from neutrons leads to the inclusion of $2\hbar\omega$ proton plus neutron configurations that mix with the $0\hbar\omega$ configurations. Inclusion of this mixing requires a

renormalization of the $0\hbar\omega$ part of the WBA-M Hamiltonian [29].

The proton configuration of the $3/2^+$ ^{27}Ne ground state is predominantly $\pi(0s_{1/2})^2\pi(0p_{1/2})^2\pi(0p_{3/2})^4\pi(0d_{5/2})^2$ and the removal of the last two protons outside the closed p shell selectively populates the $3/2^+$ ground state of ^{25}O . According to the eikonal calculations, 65% of the total two-proton removal cross section (integrated up to 10 MeV) populates the ^{25}O ground state. In order to populate excited states, it is necessary to remove protons from the core which leads to negative-parity states if one proton is removed from the p shell.

The OXBASH-eikonal calculations predict that six negative-parity states between 8.8 and 9.6 MeV are each populated with more than 3% of the ground-state population. None of the lower-energy states have populations of more than 2%. The total population of these six states sums up to about 25% of that of the ground state. This implies that over 40% of the total strength to excited states up to 10 MeV is concentrated around 9 MeV, which is consistent with the observation of resonance strength in this region.

V. SUMMARY AND CONCLUSIONS

The work presented here provides evidence for highly excited state(s) of ^{25}O located ~ 3 MeV above the three-neutron separation energy with respect to ^{22}O . This corresponds to

an excitation energy in ^{25}O of about 9 MeV. The states were populated in two-proton removal reactions from ^{27}Ne and reconstructed via invariant mass spectroscopy by measuring three neutrons in coincidence with the ^{22}O fragments. The data were modeled as sequential decay with levels in ^{25}O (3 MeV above the three-neutron separation energy), ^{24}O (700 keV), and ^{23}O (50 keV).

The population of ^{25}O excited states in the reaction $^{27}\text{Ne}(-2p)$ is dominated by the contribution where one proton is removed from the p -shell core leading to negative-parity states. OXBASH-eikonal calculations predict a significant fraction ($> 40\%$) of the excited-state population (up to 10 MeV) concentrated in a few states around an excitation energy of 9 MeV, which is consistent with the data.

ACKNOWLEDGMENTS

We would like to thank the staff of the Coupled Cyclotron Facility at the NSCL for providing the primary beam and developing the radioactive secondary beam. J.A.T. acknowledges support from the Science and Technology Facilities Council (UK) Grant No. ST/L005743/1. This work was supported by the National Science Foundation under Grants No. PHY-1306074, No. PHY-1613188, No. PHY-1102511, No. PHY-1404236, No. PHY-1713522, No. PHY-1811855, and No. PHY-1565546.

-
- [1] T. Baumann, A. Spyrou, and M. Thoennessen, *Rep. Prog. Phys.* **75**, 036301 (2012).
- [2] C. R. Hoffman, T. Baumann, D. Bazin, J. Brown, G. Christian, P. A. DeYoung, J. E. Finck, N. Frank, J. Hinnefeld, R. Howes *et al.*, *Phys. Rev. Lett.* **100**, 152502 (2008).
- [3] E. Lunderberg, P. A. DeYoung, Z. Kohley, H. Attanayake, T. Baumann, D. Bazin, G. Christian, D. Divaratne, S. M. Grimes, A. Haagsma *et al.*, *Phys. Rev. Lett.* **108**, 142503 (2012).
- [4] Y. Kondo, T. Nakamura, R. Tanaka, R. Minakata, S. Ogoshi, N. A. Orr, N. L. Achouri, T. Aumann, H. Baba, F. Delaunay *et al.*, *Phys. Rev. Lett.* **116**, 102503 (2016).
- [5] Z. Elekes, Z. Dombrádi, N. Aoi, S. Bishop, Z. Fülöp, J. Gibelin, T. Gomi, Y. Hashimoto, N. Imai, N. Iwasa *et al.*, *Phys. Rev. Lett.* **98**, 102502 (2007).
- [6] A. Schiller, N. Frank, T. Baumann, D. Bazin, B. A. Brown, J. Brown, P. A. DeYoung, J. E. Finck, A. Gade, J. Hinnefeld *et al.*, *Phys. Rev. Lett.* **99**, 112501 (2007).
- [7] K. Tshoo, Y. Satou, C. Bertulani, H. Bhang, S. Choi, T. Nakamura, Y. Kondo, S. Deguchi, Y. Kawada, Y. Nakayama *et al.*, *Phys. Lett. B* **739**, 19 (2014).
- [8] C. Hoffman, T. Baumann, D. Bazin, J. Brown, G. Christian, D. Denby, P. DeYoung, J. Finck, N. Frank, J. Hinnefeld *et al.*, *Phys. Lett. B* **672**, 17 (2009).
- [9] C. R. Hoffman, T. Baumann, J. Brown, P. A. DeYoung, J. E. Finck, N. Frank, J. Hinnefeld, S. Mosby, W. A. Peters, W. F. Rogers *et al.*, *Phys. Rev. C* **83**, 031303(R) (2011).
- [10] K. Tshoo, Y. Satou, H. Bhang, S. Choi, T. Nakamura, Y. Kondo, S. Deguchi, Y. Kawada, N. Kobayashi, Y. Nakayama *et al.*, *Phys. Rev. Lett.* **109**, 022501 (2012).
- [11] M. D. Jones, N. Frank, T. Baumann, J. Brett, J. Bullaro, P. A. DeYoung, J. E. Finck, K. Hammerton, J. Hinnefeld, Z. Kohley *et al.*, *Phys. Rev. C* **92**, 051306(R) (2015).
- [12] W. F. Rogers, S. Garrett, A. Grovom, R. E. Anthony, A. Aulie, A. Barker, T. Baumann, J. J. Brett, J. Brown, G. Christian *et al.*, *Phys. Rev. C* **92**, 034316 (2015).
- [13] M. D. Jones, K. Fosse, T. Baumann, P. A. DeYoung, J. E. Finck, N. Frank, A. N. Kuchera, N. Michel, W. Nazarewicz, J. Rotureau *et al.*, *Phys. Rev. C* **96**, 054322 (2017).
- [14] A. Volya and V. Zelevinsky, *Phys. Rev. Lett.* **94**, 052501 (2005).
- [15] National Nuclear Data Center, Brookhaven National Laboratory; ENSDF and XUNDL databases, <https://www.nndc.bnl.gov/>.
- [16] G. Hagen, M. Hjorth-Jensen, G. R. Jansen, and T. Papenbrock, *Phys. Scr.* **91**, 063006 (2016).
- [17] K. Hagino and H. Sagawa, *Phys. Rev. C* **93**, 034330 (2016).
- [18] A. N. Kuchera, A. Spyrou, J. K. Smith, T. Baumann, G. Christian, P. A. DeYoung, J. E. Finck, N. Frank, M. D. Jones, Z. Kohley *et al.*, *Phys. Rev. C* **91**, 017304 (2015).
- [19] M. D. Jones, Z. Kohley, T. Baumann, G. Christian, P. A. DeYoung, J. E. Finck, N. Frank, R. A. Haring-Kaye, A. N. Kuchera, B. Luther *et al.*, *Phys. Rev. C* **91**, 044312 (2015).
- [20] M. D. Jones, Ph.D. Thesis, Spectroscopy of neutron unbound states in ^{24}O and ^{23}N , Michigan State University, 2015.
- [21] H. Ryuto, M. Kunibu, T. Minemura, T. Motobayashi, K. Sagara, S. Shimoura, M. Tamaki, Y. Yanagisawa, and Y. Yano, *Nucl. Instrum. Methods Phys. Res., Sect. A* **555**, 1 (2005).
- [22] N. Frank, A. Schiller, D. Bazin, W. Peters, and M. Thoennessen, *Nucl. Instrum. Methods Phys. Res., Sect. A* **580**, 1478 (2007).

- [23] K. Makino and M. Berz, *Nucl. Instrum. Methods Phys. Res., Sect. A* **558**, 346 (2006).
- [24] S. Agostinelli, J. Allison, K. Amako, J. Apostolakis, H. Araujo, P. Arce, M. Asai, D. Axen, S. Banerjee, G. Barrand *et al.*, *Nucl. Instrum. Methods Phys. Res. Sect. A* **506**, 250 (2003).
- [25] B. Roeder, Development and validation of neutron detection simulations for EURISOL, EURISOL Design Study, Report No. 10-25-2008-006-In-beamvalidations.pdf, 2008, p. 31, http://ns.ph.liv.ac.uk/eurisol/M3_in-beam_validations.pdf.
- [26] J. A. Tostevin and B. A. Brown, *Phys. Rev. C* **74**, 064604 (2006).
- [27] B. Brown, A. Etchegoyen, W. Rae, and N. Godwin, MSU-NSCL Report No. 524, 1988.
- [28] B. Brown and W. Rae, *Nucl. Data Sheets* **120**, 115 (2014).
- [29] A. Lepailleur, K. Wimmer, A. Mutschler, O. Sorlin, J. C. Thomas, V. Bader, C. Bancroft, D. Barofsky, B. Bastin, T. Baugher *et al.*, *Phys. Rev. C* **92**, 054309 (2015).